# Direct observation of the phonon dispersion of a three-dimensional solid/solid hypersonic colloidal crystal

Gaohua Zhu,[1,*] Nichlas Z. Swinteck,[2] Songtao Wu,[1] Jin S. Zhang,[3] Huihui Pan,[3] Jay D. Bass,[3] Pierre A. Deymier,[2] Debasish Banerjee,[1] and Kazuhisa Yano[1,4,*]

[1]*Materials Research Department, Toyota Research Institute of North America, Ann Arbor, Michigan 48105, USA*

[2]*Department of Materials Science and Engineering, University of Arizona, Tucson, Arizona 85721, USA*

[3]*Department of Geology, University of Illinois at Urbana-Champaign, Urbana, Illinois 61801, USA*

[4]*Inorganic Materials Laboratory, Toyota Central R&D Labs. Inc, Nagakute, Aichi 480-1192, Japan*

(Received 6 August 2013; revised manuscript received 30 September 2013; published 22 October 2013)

We report on Brillouin measurements of the phonon dispersion relation of a three-dimensional hypersonic phononic crystal. The phononic crystal, comprised of close-packed polystyrene spheres embedded in a background matrix of solid polydimethylsiloxane, was fabricated using a self-assembly technique. The experimentally measured dispersion relation reveals the band folding effect and the formation of a band gap for longitudinal waves at the boundary of the Brillouin zone. Theoretical calculations, based on the finite element method and the finite-difference time-domain method, are employed to interpret experimentally observed phonon modes and provide insight on important features of the solid/solid hypersonic crystals.

DOI: 10.1103/PhysRevB.88.144307 PACS number(s): 62.30.+d, 78.35.+c

Phononic crystals, with periodic variation in the density and elastic properties, can exhibit forbidden bands in their acoustic transmission spectrum. This type of material prevents elastic wave propagation in certain frequencies and could be used to manipulate the propagation of acoustic waves by engineering the phonon band structure.[1–6] In the past, research has been focused on sonic and ultrasonic phononic crystals.[4,7–9] With the recent advances in material fabrication and characterization techniques, phononic crystal research has been extended to the hypersonic frequency region ($10^9$–$10^{12}$ Hz).[10–13] Hypersonic phononic crystals are nanocomposites with periodic structures. Because of its submicrometer structures, hypersonic crystals can coherently scatter both visible light (photons) and acoustic waves (phonons). More interestingly, the ability of hypersonic crystals to influence high frequency phonons offers a unique opportunity to manipulate physical properties, such as heat capacity and thermal conductivity.[12,13]

Direct observation of phononic dispersion in the hypersonic frequency regime was realized experimentally by using Brillouin light scattering (BLS) first in the two-dimensional (2D) epoxy-based phononic crystals,[14,15] and later in the three-dimensional (3D) close-packed polymer colloidal systems.[16,17] In previous works, the phononics are solid/fluid systems consisting of periodically arranged solid inclusions surrounded by a fluid with similar refractive index to that of the solid. The index-matching liquid is used to reduce strong multiple light scattering caused by the large contrast in the refractive index between the solid inclusions and surrounding air.[14–18] Because of the complexity associated with band structures for solid/solid systems, very few attempts have been made to experimentally characterize dispersion relations for systems comprised entirely of solid constituents. However, these studies are limited to 1D or 2D systems.[14,15,19] Quantitative evaluation of the phonon dispersion with experimental BLS data remains an open challenging problem, and it necessitates the use of additional tools to help understand the modes supported in phononic crystals.[17] Specifically, numerical tools such as the finite element (FE) and finite-difference time-domain (FDTD) methods offer tremendous insights on the phonon dispersion relations as well as transmission spectra, and can assist greatly in the elucidation of BLS spectra of the phononic crystals.

In this study, we fabricate 3D solid/solid colloidal hypersonic phononic crystals using the self-assembly method. The polystyrene (PS) spheres were aligned in face-centered-cubic (fcc) structure, and then embedded in the background matrix of homogeneous polydimethylsiloxane (PDMS). The phonon band structure was experimentally characterized by BLS without infiltration of any index-matching liquid. The measured phonon band structure features a band gap at the boundary of the first Brillouin zone. The FE and FDTD calculations for the phonon dispersion diagram and transmission spectrum of the phononic crystal are utilized to explain experimental BLS spectra.

Monodispersed colloidal PS spheres (Bangs Laboratories, Inc.) with a nominal diameter of 215 $\pm$ 10 nm were assembled on a quartz substrate using a modified evaporation-induced self-assembly (EISA) method.[20] After a Piranha clean, the hydrophilic substrate was placed at a 30° angle in a 20 ml vial with 2 ml PS dispersion (1.0 wt.%) in deionized water. The vial was left inside a vibration-free, temperature controlled incubator at 35 °C for 3 days to dry the aqueous dispersion to form a thin film of close-packed PS spheres on the substrate. The PS film was then infiltrated with premixed PDMS elastomer precursor, Sylgard 184 (Dow Corning), which was diluted in silicon fluid DMS-T00 (Gelest). The gaps between PS spheres were completely filled with liquid PDMS through capillary force. The film was cured at room temperature for one night, followed by additional hardening for 6 h at 55 °C.[21] The as-prepared specimen is comprised of monodispersed PS spheres arranged in face-centered-cubic (fcc) structure in a background matrix of solid PDMS with (111) surfaces orientated parallel to the substrate. The thickness of the middle area of the sample, which is used for all BLS measurements, is approximately 10 $\mu$m. The quality of the specimen was characterized by spectrophotometry and scanning electron

 

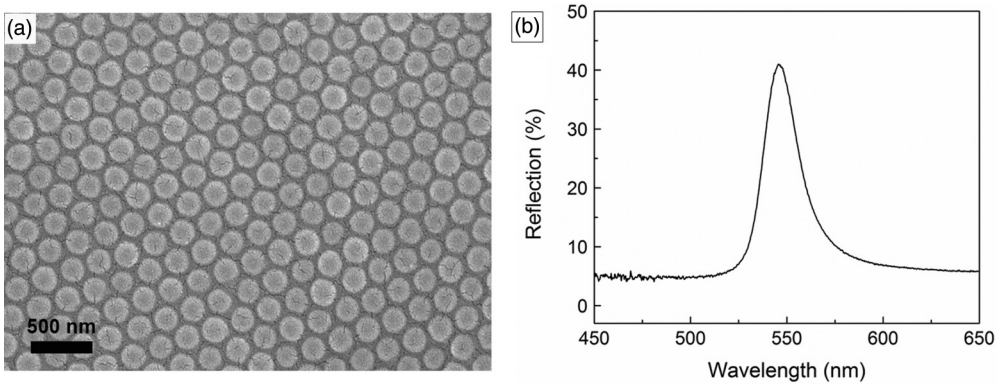


FIG. 1. (a) SEM top-view image of the PS/PDMS phononic crystal; (b) reflection spectrum at an incidence angle of 8°.

microscopy (SEM). The top view of a PS/PDMS specimen in Fig. 1(a) shows excellent uniformly ordered structure in a plane oriented parallel to the substrate and the gaps between the PS spheres are filled with PDMS. The estimated center-to-center distance between the PS spheres is 217 nm as indicated by the SEM image. The reflection spectrum, obtained at near normal incidence angle ($\theta = 8°$) to the (111) surface of specimen, shows a clear first-order diffraction peak at $\lambda_{max} = 546$ nm [Fig. 1(b)]. Assuming PS spheres are aligned in fcc structure, the diameter of a PS sphere estimated from the constructive interference condition [Eq. (1)]

$$\lambda_{max} = \sqrt{\frac{8}{3}}\varphi\sqrt{n_{eff}^2 - \sin^2\theta} \qquad (1)$$

is about 226 nm, where $\varphi$ is the PS sphere diameter, $\theta = 8°$ the incidence angle, and $n_{eff} = 1.54$ the effective refractive index of the PS/PDMS crystal. Results from both SEM and reflection spectrum are consistent with the actual PS sphere size, indicating PS spheres are close packed with good crystallinity.

The measurement of the phonon band structure was performed by BLS. BLS is a nondestructive, noncontact technique that utilizes the physics of inelastic photon-phonon scattering phenomena to characterize hypersonic phonon modes in materials with submicrometer characteristic length scales. Compared to inelastic neutron or x-ray scattering techniques, BLS offers a much higher frequency resolution.[22–24] Such high resolution is achieved by the use of a six-pass tandem Fabry-Pérot interferometer. For this study, an angle-resolved BLS system (Fig. 2) was built to allow the scattering angle to be changed continuously to any desired angle up to near backscattering angle ($\theta_{max} = 141°$). A compact diode-pumped solid-state laser with wavelength $\lambda$ of 532 nm was installed on the $2\theta$ arm in the system with as the *X-Y-Z* translational sample stage was installed in the center of a $2\theta$-rotational stage. Brillouin spectra were recorded using symmetric transmission scattering geometry. Phonon wave vectors measured with

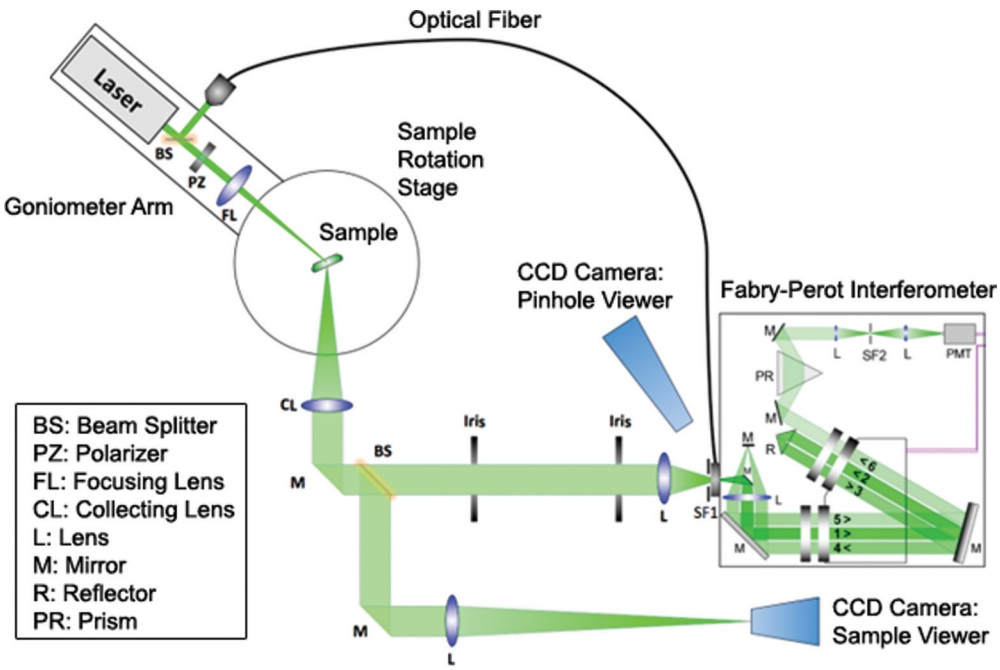


FIG. 2. (Color online) Schematic of the homebuilt angle-resolved Brillouin light scattering system.

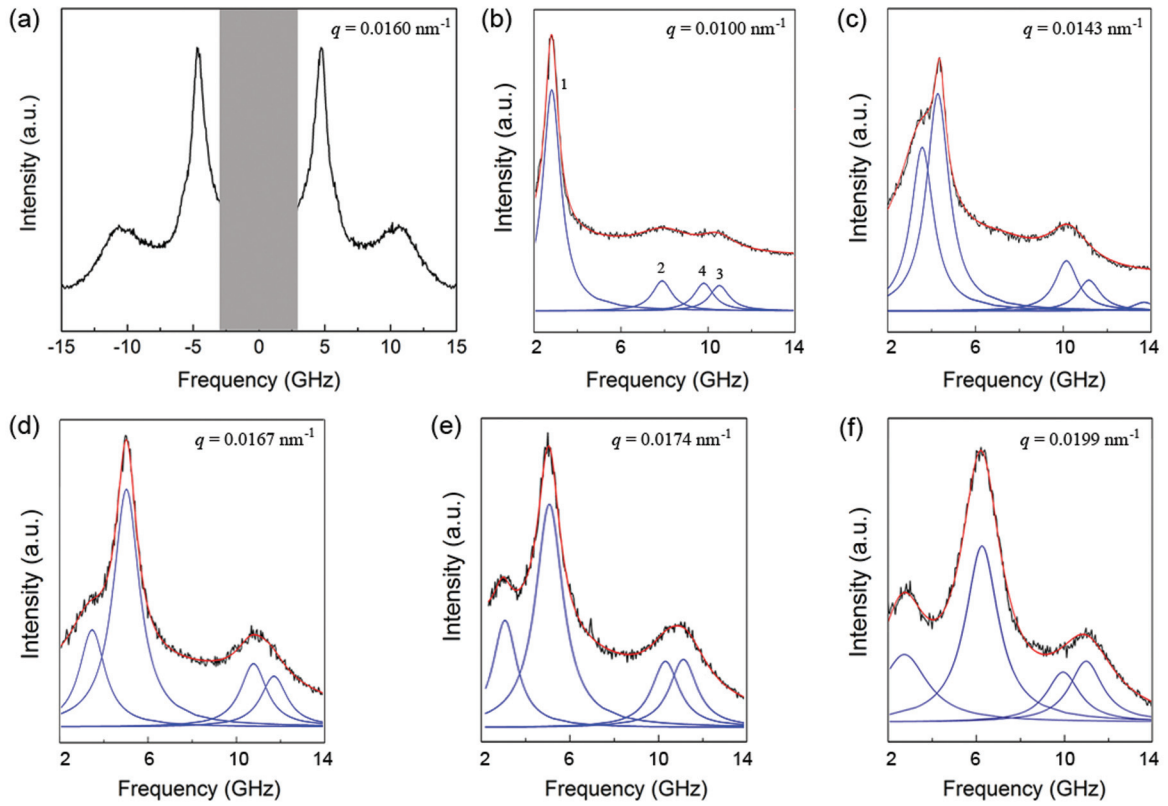


FIG. 3. (Color online) (a) Typical Brillouin spectrum for $q = 0.0160\ \text{nm}^{-1}$; (b)–(f) BLS spectra recorded at various scattering angles. The anti-Stoke side of the observed Brillouin spectra are reproduced by Lorentzian functions (blue lines).

transmission BLS reside in the (111) plane of the phononic crystal film.[16] Conservation of momentum insists the following wave vector relationship: $\boldsymbol{q} = \boldsymbol{k}_s - \boldsymbol{k}_i$, where $\boldsymbol{q}$, $\boldsymbol{k}_s$, and $\boldsymbol{k}_i$ respectively denote wave vectors for the scattered photon and the incident photon. $\boldsymbol{k}_s$ and $\boldsymbol{k}_i$ can be regarded as of equal magnitude. Therefore, $\boldsymbol{q}$ is determined by the following equation,

$$\boldsymbol{q} = \frac{4\pi}{\lambda}\sin\left(\frac{\theta}{2}\right), \tag{2}$$

where $\theta$ is the scattering angle. The dispersion relations were measured by varying the scattering angle $\theta$ to probe phonon wave vectors up to the second Brillouin zone.

In solid/solid phononic crystals, longitudinal and transverse phonon waves are usually coupled together. By using different incident and scattered light polarizations, the longitudinal and transverse phonon modes can be measured separately.[25] In this work, only longitudinal phonon modes from the PS/PDMS specimen were recorded in Brillouin spectra. The transverse signals from the self-assembled colloidal specimen cannot be observed clearly, which can be attributed to the low contrast between PS and surrounding PDMS. Figure 3(a) shows a typical Brillouin spectrum for wave vector $q = 0.0160\ \text{nm}^{-1}$, which was recorded at scattering angle $\theta = 85^\circ$. The frequencies of the phonon peaks were obtained by fitting the Brillouin spectra with Lorentzian functions. For example, as shown in Fig. 3(b), the most intense Brillouin signal corresponds to the longitudinal acoustic phonon mode for peak (1) at 2.84 GHz. Less intense peaks can be fit using three Lorentzian functions (2), (3), and (4) at 8.02, 9.64, and 10.81 GHz, respectively. Peaks at 8.02 and 10.81 GHz are contributed by various higher order vibrational modes, whereas the weak peak at 9.64 GHz is the longitudinal phonon signal which comes from the quartz substrate.

Figures 3(b)–3(f) show the anti-Stokes side of Brillouin spectra recorded at various scattering angles in the range of $0.0100\ \text{nm}^{-1} \leqslant q \leqslant 0.0199\ \text{nm}^{-1}$. Phonon eigenfrequencies are obtained by fitting the peaks in each spectrum with Lorentzian functions. It is clearly presented that the shape of the major Brillouin scattering signal evolves from a single peak at low wave vector $q$ to double peaks when $q$ approaches the vicinity of the Brillouin zone boundary. Such a change in the Brillouin spectra shape is clear evidence of the formation of a phononic band gap at the boundary of the first Brillouin zone. The experimentally measured phonon dispersion relations are plotted in Fig. 4(a), where frequencies of the phonon modes are plotted as a function of phonon wave vector $q$. The dispersionless modes ($\omega = kc$) in solid circles are the experimentally measured longitudinal acoustic phonons from the quartz substrate. The dashed blue line indicates the longitudinal phonon propagation in the substrate, and it matches the BLS data very well. Solid red diamonds are the eigenfrequency modes supported by the PS/PDMS specimen. The experimental phonon dispersion of the PS/PDMS specimen is nearly linear at low frequency, and then bended significantly when approaching the boundary of

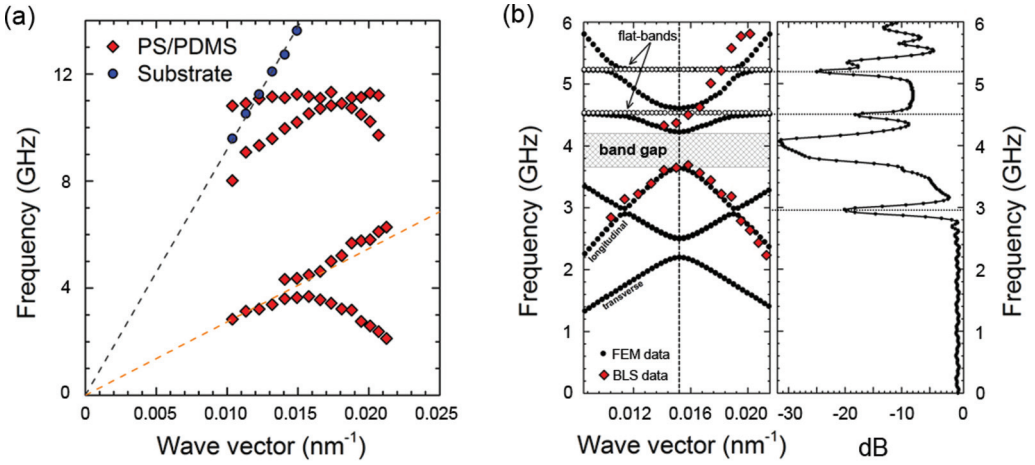


FIG. 4. (Color online) (a) Experimental phononic dispersion relation shows a band gap between 3.7 and 4.4 GHz. Solid red diamonds, phonon crystal modes from PS/PDMS crystal; solid blue circles, phonon modes from the quartz substrate; dashed blue line: theoretical acoustic phonon propagation in the substrate; dashed orange line: acoustic phonon propagation in a homogeneous effective medium of PS/PDMS. (b) A FE computed phononic dispersion superposed with BLS data (left) and a transmission spectrum simulated by FDTD (right).

the Brillouin zone, forming a Bragg gap with a gap width of about 0.7 GHz. The dashed orange line in Fig. 4(a) represents a linear fit to these data points. The slope of this line corresponds to the effective speed of sound for the PS/PDMS composite, which is approximately equal to 1721 m/s. This value can be well estimated by using Wood's law [Eq. (3)],[26]

$$\frac{1}{\rho_{\text{eff}} c_{\text{eff}}^2} = \frac{\varphi_{\text{PS}}}{\rho_{\text{PS}} c_{\text{PS}}^2} + \frac{\varphi_{\text{PDMS}}}{\rho_{\text{PDMS}} c_{\text{PDMS}}^2}, \tag{3}$$

where $\rho$, $c$, *and* $\varphi$ are mass density, sound velocity, and volume percentage with the effective density $\rho_{\text{eff}} = \varphi_{\text{PS}}\rho_{\text{PS}} + \varphi_{\text{PDMS}}\rho_{\text{PDMS}}$.

In order to better understand the phonon modes measured by BLS, theoretical simulations using FE and FDTD methods were carried out to calculate the phonon dispersion relations and transmission spectra along particular directions of symmetry in fcc reciprocal space. For both numerical techniques, the solid/solid PS/PDMS phononic crystal is modeled as an elastic composite body comprised of a fcc arrangement of homogeneous PS spheres in a background matrix of solid homogeneous PDMS. Band structure calculations are computed for a crystal of infinite extent in all spatial directions, whereas transmission calculations use a finite slab of the phononic crystal which consists of 10 layers of PS along the $\Gamma$-$L$ direction. In our calculations, PS spheres ($\varphi = 215$ nm) occupy 72% of the volume associated with the unit cell of a fcc crystal, which is a good approximation of our actual specimen. Material properties used in theoretical calculations are $\rho_{\text{PS}} = 1060\ \text{kg/m}^3$, $C_{L,\text{PS}} = 2350$ m/s, $C_{T,\text{PS}} = 1230$ m/s, $\rho_{\text{PDMS}} = 965\ \text{kg/m}^3$, $C_{L,\text{PDMS}} = 1190$ m/s, and $C_{T,\text{PDMS}} = 500$ m/s, where $\rho$, $C_L$, and $C_T$ represent density, longitudinal speed of sound, and transverse speed of sound, respectively. It is found that FE calculated band structure shows numerous localized resonance modes (flat bands). We interpret these bands as resonance modes confined to the small pocket of PDMS located in between PS spheres. The frequencies of such localized resonance modes increase dramatically with increasing $C_{T,\text{PDMS}}$. Since the longitudinal acoustic branch is insensitive to the value used for $C_{T,\ \text{PDMS}}$, by selecting $C_{T,\text{PDMS}} = 500$ m/s, the position of the lowest flat band can be pushed above the longitudinal acoustic branch in the dispersion relation diagram. This approach allows us to study the position of the longitudinal acoustic branch in the dispersion diagram and relate band gap information to BLS results.

The experimental phonon dispersions are superposed onto the theoretical band structure computed by FE and plotted in Fig. 4(b). The theoretical band structures are calculated along the $\Gamma$-$L$ direction, and the measured phonon wave vector resides in the (111) plane. Given the band splitting is roughly constant near Brillouin zone face centers as suggested by first-order perturbation theory, it is a good approach to compare the BLS measurements with the theoretical phonon dispersions along the $\Gamma$-$L$ direction in order to interpret the phonon propagation modes and band gap.[16,27,28] The band structure simulated by FE calculations shows that the longitudinal branch stems from the $\Gamma$ point and folds at the boundary of the Brillouin zone, forming a phononic band gap in the range of 3.7–4.2 GHz at the $L$ point, which is identified with a vertical dashed line in Fig. 4(b). There is a clear overlap in frequency between the gap observed in the BLS experiment and the gap determined by FE. The transmission spectrum of the longitudinal wave simulated by FDTD along the $\Gamma$-$L$ direction is presented on the left of Fig. 4(b). The forbidden bands indicated by the minimums in the transmission spectrum are consistent with the FE calculations and the experimental results. In addition, FE calculations show two flat bands in the band structure in Fig. 4(b), one occurring at 4.6 GHz and the other at 5.2 GHz, which can be attributed to the resonance modes of the PS opals. The lowest and most intense (1,2) resonance mode lies within the Bragg gap and is not shown in Fig. 4(b). The frequency downshift for these flat bands can be caused by the soft surrounding PDMS matrix. As a result of hybridization, hybridization gaps open up and avoid crossing of the flat bands and longitudinal branch.[29,30] The apparent absence of these hybridization gaps in the experimental dispersions could be due to the weak

coupling between the PS spheres and soft polymer matrix, making it difficult to observe such hybridization gaps in BLS measurements.[16,17]

High frequency phonon modes (>8 GHz), which have never been reported in solid/liquid systems before, were observed as well in our solid/solid PS/PDMS system. However, compared to the low frequency modes, these high frequency phonon modes are strongly mixed, and the scattering signals are usually very weak. Besides, some high frequency modes may not be observed in BLS even after a very long accumulation time.[14] Therefore, all these factors combined makes it challenging to match the high frequency experimental BLS data with the simulation results.

In summary, we investigated the phonon dispersion relation of a fcc structured phononic crystal consisting of PS spheres in a solid PDMS matrix. The phonon band structure measured by BLS shows a band gap and band-folding effect at the boundary of the first Brillouin zone, which can be attributed to coherent scattering by phononic crystal structure. We used FE and FDTD methods to perform phonon band structure and transmission spectrum simulations, respectively, for the 3D PS/PDMS phononic crystal, and obtained good agreement with the experimental BLS data. While the BLS results are qualitatively similar to those observed in solid/liquid phononic crystals, solid/solid phononic crystals have a significant advantage in design of practical hypersonic devices. Furthermore, the demonstration of the agreement between experiment and theory at the submicron scale opens the prospect of further development of 3D solid/solid hypersonic phononic crystal systems.

*Authors to whom correspondence should be addressed: gaohua.zhu@tema.toyota.com; k-yano@mosk.tytlabs.co.jp

[1]M. S. Kushwaha, P. Halevi, L. Dobrzynski, and B. Djafari-Rouhani, Phys. Rev. Lett. **71**, 2022 (1993).
[2]Z. Liu, X. Zhang, Y. Mao, Y. Y. Zhu, Z. Yang, C. T. Chan, and P. Sheng, Science **289**, 1734 (2000).
[3]J. H. Page, A. Sukhovich, S. Yang, M. L. Cowan, F. Van Der Biest, A. Tourin, M. Fink, Z. Liu, C. T. Chan, and P. Sheng, Phys. Status Solidi B **241**, 3454 (2004).
[4]J. O. Vasseur, P. A. Deymier, B. Chenni, B. Djafari-Rouhani, L. Dobrzynski, and D. Prevost, Phys. Rev. Lett. **86**, 3012 (2001).
[5]A. Sukhovich, B. Merheb, K. Muralidharan, J. O. Vasseur, Y. Pennec, P. A. Deymier, and J. H. Page, Phys. Rev. Lett. **102**, 154301 (2009).
[6]T. Gorishny, M. Maldovan, C. K. Ullal, and E. L. Thomas, Phys. World **18**, 24 (2005).
[7]S. Yang, J. H. Page, Z. Liu, M. L. Cowan, C. T. Chan, and P. Sheng, Phys. Rev. Lett. **88**, 104301 (2002).
[8]F. R. Montero de Espinosa, E. Jimenez, and M. Torres, Phys. Rev. Lett. **80**, 1208 (1998).
[9]N. Swinteck, J. O. Vasseur, A. C. Hladky-Hennion, C. Croenne, S. Bringuier, and P. A. Deymier, J. Appl. Phys. **112**, 024514 (2012).
[10]L. Dhar and J. A. Rogers, Appl. Phys. Lett. **77**, 1402 (2000).
[11]U. Ozgur, C. W. Lee, and H. O. Everitt, Phys. Rev. Lett. **86**, 5604 (2001).
[12]P. E. Hopkins, C. M. Reinke, M. F. Su, R. H. Olsson III, E. A. Shaner, Z. C. Leseman, J. R. Serrano, L. M. Phinney, and I. El-Kady, Nano Lett. **11**, 107 (2011).
[13]J. Yu, S. Mitrovic, D. Tham, J. Varghese, and J. R. Heath, Nat. Nanotechnol. **5**, 718 (2010).
[14]T. Gorishnyy, C. K. Ullal, M. Maldovan, G. Fytas, and E. L. Thomas, Phys. Rev. Lett. **94**, 115501 (2005).
[15]T. Gorishnyy, J. Jang, C. Y. Koh, and E. L. Thomas, Appl. Rev. Lett. **91**, 121915 (2007).
[16]W. Cheng, J. Wang, U. Jonas, G. Fytas, and N. Stefanou, Nat. Mater. **5**, 830 (2006).
[17]T. Still, W. Cheng, M. Retsch, R. Sainidou, J. Wang, U. Jonas, N. Stefanou, and G. Fytas, Phys. Rev. Lett. **100**, 194301 (2008).
[18]J. H. Jang, C. Y. Koh, K. Bertoldi, M. C. Boyce, and E. L. Thomas, Nano Lett. **9**, 2113 (2009).
[19]D. Schneider, F. Liaqat, E. H. El Boudouti, Y. El Hassouani, B. Djafari-Rouhani, W. Tremel, H. Butt, and G. Fytas, Nano Lett. **12**, 3101 (2012).
[20]P. Jiang, J. F. Bertone, K. S. Hwang, and V. L. Colvin, Chem. Mater. **11**, 2132 (1999).
[21]H. Fudouzi and Y. Xia, Langmuir **19**, 9653 (2003).
[22]R. S. Penciu, H. Kriegs, G. Petekidis, G. Fytas, and E. N. Economou, J. Chem. Phys. **118**, 5224 (2003).
[23]S. M. Lindsay, M. W. Anderson, and J. R. Sandercock, Rev. Sci. Instrum. **52**, 1478 (1981).
[24]H. Kriegs, W. Steffen, G. Fytas, G. Monaco, C. Dreyfus, P. Fragouli, M. Pitskalis, and N. Hadjichristidis, J. Chem. Phys. **121**, 2376 (2004).
[25]T. Gorishnyy, Ph.D. thesis, Massachusetts Institute of Technology, 2007.
[26]A. B. Wood, *A Textbook of Sound* (The MacMillan Co., New York, 1955).
[27]T. Still, G. Gantzounis, D. Kiefer, G. Hellmann, R. Sainidou, G. Fytas, and N. Stefanou, Phys. Rev. Lett. **106**, 175505 (2011).
[28]N. W. Ashcroft and N. D. Mermin, *Solid State Physics* (Saunders College Publishing, New York, 1976).
[29]A. A. Maznev and A. G. Every, J. Appl. Phys. **106**, 113531 (2009).
[30]I. E. Psarobas, A. Modinos, R. Sainidou, and N. Stefanou, Phys. Rev. B **65**, 064307 (2002).